



## GEOSCIENCES

# Combined performance of September's Weddell sea ice extent, Southern Annular Mode, and Atlantic SST anomalies over the South American temperature and precipitation

FERNANDA C. VASCONCELLOS, FÁBIO G. OLIVA, RENAN M. PIZZOCHERO, TELMA M. DA SILVA, CLÁUDIA K. PARISE & CATHARINE F. DE CALDAS

**Abstract:** This paper aims to analyze the relationships among tropical (Atlantic Meridional Mode - AMM), subtropical (South Atlantic Subtropical Gradient - SASG), and extratropical (Southern Annular Mode - SAM) teleconnection patterns, the Weddell Sea (WS) sea ice extents, and the climate in South America. Warm anomalies are observed in most of South America for maximum WS ice extent combinations (negative SAM/positive AMM and negative SAM/positive SASG composites), with an opposite signal at tropical South America for minimum WS ice extent combinations (positive SAM/negative AMM and positive SAM/negative SASG). Over Southern Argentina, colder (warmer) temperatures are seen at the negative SAM/positive SASG (positive SAM/negative SASG). Drier (wetter) conditions are found over most South America at maximum (minimum) WS ice extent combinations. Wavetrains from different Pacific and Indian Oceans regions are related to high-level anomalous cyclonic (anticyclonic) circulation over the continent at maximum (minimum) WS ice extent configuration, which explains the climate impacts found. The SASG signal displaces the anomaly circulations eastward from South America, impacting the adjacent Atlantic Ocean region more intensely concerning the other modes. The results discussed here indicated that these patterns (SAM, AMM, SASG, and sea ice extent) have significant links with the South American climate variability.

**Key words:** Antarctic sea ice, variability modes, South America, precipitation, temperature.

## INTRODUCTION

Climate links between the Antarctic sea ice (ASI) extremes, the atmospheric circulation, and the climate of South America have been intensely investigated in the last decades due to the importance of ASI in the balance of the global climate system by controlling the atmospheric circulation in Southern Hemisphere (Carvalho et al. 2005, Lefebvre & Goosse 2005, Pezza et al. 2008, 2012, Reboita et al. 2009, Silvestri & Vera 2009, Parise et al. 2015, Carpenedo & Ambrizzi 2016, Oliva et al. 2021). This significant impact of ASI on the climate of the Southern Hemisphere occurs since the atmosphere functions as a heat engine, characterized by excessive heating in the tropics and cooling in the high latitudes (Raphael et al. 2011, Carpenedo & Ambrizzi 2016). Antarctica represents an excellent heat sink for the planet and the Southern Hemisphere, controlling atmospheric circulation in the middle and high latitudes. The coverage ASI influences many meteorological processes, given its high reflectivity or

albedo, low thermal conductivity or insulating effect, and heat and mass exchanges with the ocean and atmosphere (Budd et al. 1989).

The ASI variability modulates the Equator-to-Pole temperature gradients, changing the southern heat transport and consequently the local, regional, and global climate (Carpenedo et al. 2013, Parise et al. 2015, Carpenedo & Ambrizzi 2016, Morioka et al. 2017). Some studies have shown the complexity and the relevance of the cryosphere-atmosphere interactions (Hall & Visbeck 2002, Cunningham & Bonatti 2011, Raphael et al. 2011, Parise et al. 2015, Comiso et al. 2017, Lima & Carvalho 2017). Other works also discussed links between ASI and the climate variability modes, such as the Southern Annular Mode (Pezza et al. 2008, 2012, Clem & Fogt 2013, Parise et al. 2015, Clem et al. 2016, Fogt & Marshall 2020, Oliva et al. 2021), the Atlantic Meridional Mode (AMM - Oliva et al. 2021), and the South Atlantic Subtropical Gradient (SASG - Oliva et al. 2021). This last one is similar to the South Atlantic Subtropical Dipole (SASD - e.g., Venegas et al. 1997, Fauchereau et al. 2003, Sterl & Hazeleger 2003, Hermes & Reason 2005, Morioka et al. 2011, Wainer et al. 2014, but with a focus on the subtropical/extratropical Atlantic. Based on Sterl & Hazeleger (2003) definition, the SASD is formed by a dipole of SST anomalies: a Northeast pole and a Southwest pole, both in the Subtropical Atlantic. According to Venegas et al. (1997), this dipole pattern is the leading mode of ocean-atmosphere coupled variability in the Subtropical Atlantic. The formation of SASD is related to pressure and wind anomalies. According to Sterl & Hazeleger (2003), the pressure anomalies centered at 15°W and 45°S are connected to the SST anomalies, since the anomalous winds associated with the pressure are responsible for SST anomalies through latent heat flux anomalies and changes in the thickness of the mixing layer (Morioka et al. 2011).

Oliva et al. (2021) examined the links between these teleconnection patterns phases and the Weddell Sea sector (WS) sea ice. Their results have shown the negative SAM/positive AMM phase and the negative SAM/positive SASG phase combinations were associated with maximum ASI extents. The opposite combinations of these indices were related with minimum ASI extents. Other studies also pointed to the influence of some teleconnection patterns on South America variability (e.g., Reboita et al. 2009, Bombardi et al. 2014, Jorgetti et al. 2014, Vasconcellos et al. 2019, Caldas et al. 2020, Vasconcellos & Souza 2022). In this context, this paper aims to complement these results, evaluating the impacts of the combination of these variability modes and the WS ice, as discussed in detail in Oliva et al. (2021), over the South American climate variability. The following three questions were here investigated:

1. Are SAM, AMM, and SASG combinations related to extreme WS ice extents during September?
2. Based on this, what are the impacts of these combinations on South American air temperature and precipitation anomalies?
3. What are the possible mechanisms linking these variability modes, the WS ice extent, and the South American climate?

## **MATERIALS AND METHODS**

### **Datasets**

We used monthly climate data from January 1981 to December 2018, 38 years.

The ASI concentration data were obtained from the National Snow and Ice Data Center (NSIDC) from Nimbus-7 SMMR and DMSP SSM/I-SSMIS, version 3 (available in <https://nsidc.org/data/NSIDC-0079/versions/3>) satellite dataset. The data are organized in a stereographic polar grid in a grid cell with pixels with a horizontal spacing of 25 km x 25 km. More information about this dataset is given in Comiso (2017).

The precipitation dataset was obtained from the Global Precipitation Climatology Project (GPCP), with a spatial resolution of 2.5° Lat/Lon. These data are derived from surface observations and estimated precipitation by microwave channels from low-earth orbit satellites and infrared channels from geostationary orbit satellites. Further information about GPCP can be found in Adler et al. (2003).

The atmospheric data of geopotential height at 700 hPa and 250 hPa, 2m air temperature, sea level pressure (SLP), and wind at 850 and 250 hPa were obtained from the European Centre for Medium-Range Weather Forecasts (ECMWF) ERA-Interim Reanalysis, with a spatial resolution of 0.75° Lat/Lon (Dee et al. 2011).

The National Oceanic and Atmospheric Administration (NOAA) Extended Reconstructed Sea Surface Temperature dataset, version 5 (ERSSTv5), was used. It is a global monthly SST data derived from the International Comprehensive Ocean-Atmosphere Dataset (ICOADS). The horizontal resolution of ERSSTv5 is 2° Lat/Lon, with improved spatial completeness using statistical methods. Further details can be found in Huang et al. (2017).

This study used the AMM index from the National Centers for Environmental Prediction/National Center for Atmospheric Research (NCEP/NCAR) Reanalysis monthly data, which describes the principal mode of variability in the Tropical Atlantic Ocean. The data are defined over the region (21°S – 32°N, 74°W – 15°E) and spatially smoothed (three longitudes by two latitude points) to identify the spatial pattern. Data are available at <http://www.esrl.noaa.gov/psd/data/timeseries/monthly/AMM/>. More details can be found in Chiang & Vimont (2004).

## Methods

To calculate the total area of ASI concentration, we used the software MatLab, version R2016a. We attributed value 1 to the pixels that represent sea ice concentration above or at least 15% and value zero to the pixels with sea ice concentration below 15%. The sea ice concentration total area is calculated by counting the number of pixels with value 1 and multiplying the obtained value by the total area occupied by each pixel (625 km<sup>2</sup>). The total area of sea ice concentration is given in km<sup>2</sup> (Gloersen et al. 1992).

To calculate the ASI extent (km) to each longitude, we considered the distance between the continent edge latitude and the sea ice edge latitude. The horizontal grid (Longitude vs. Latitude) was obtained from the NSIDC webpage. Then, we found the circle arch between these two grid points (in degrees) and converted the circle arch value to kilometers by using the MatLab functions of distance and deg2km. Due to its broad coverage of ASI and its proximity to South America, this study focused on the western WS sector (from 60°W - 0°) - Figure 1. The WS reaches up to 20°E longitude (Cavaliere & Parkinson 2008). We also identified the first (for minimum condition) and fifth (for maximum condition) quintiles of WS ice extent (km).

The monthly SAM index used in this work was calculated applying the Empirical Orthogonal Function (EOF) method on the geopotential height anomalies at 700 hPa for the area from 30°S to

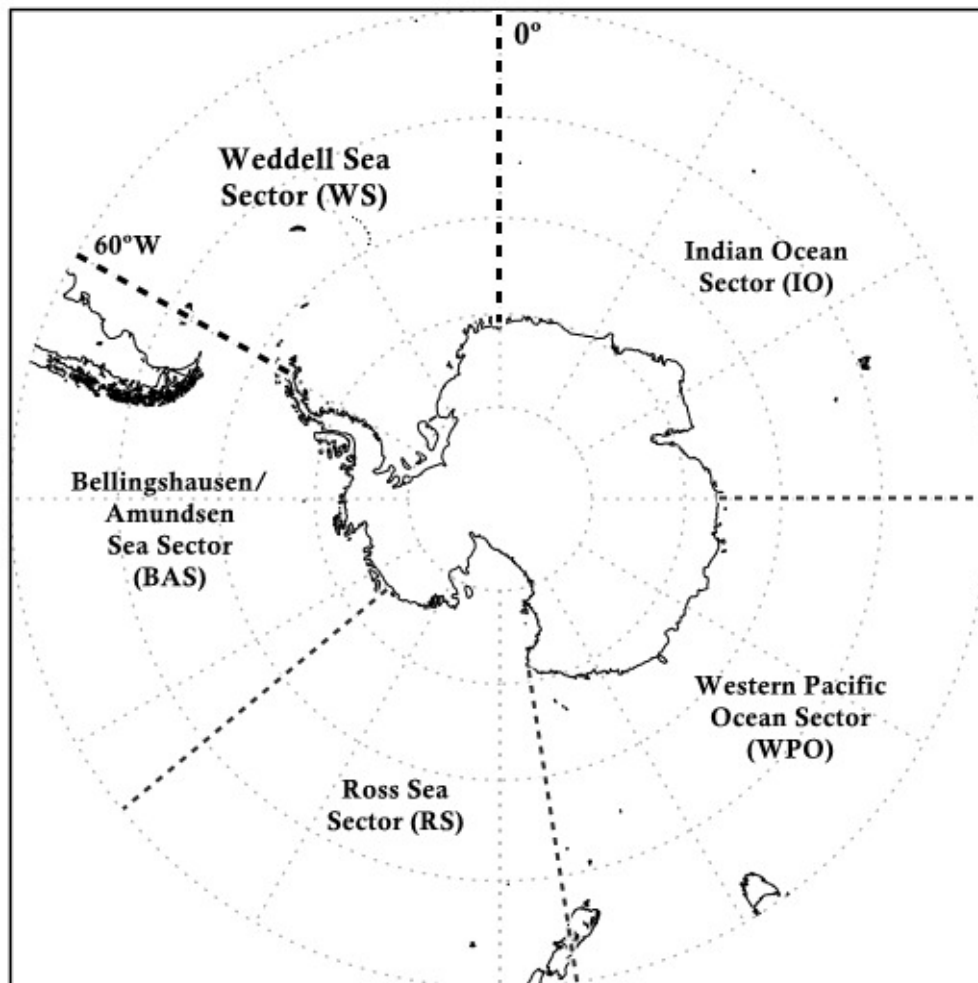


**Figure 1.** Southern Ocean sectors, emphasizing the WS sector ( $60^{\circ}\text{W} - 0^{\circ}$ ), delimited by thick dashed lines.

$90^{\circ}\text{S}$  (Vasconcellos et al. 2019). The region used for calculating the EOF differs from that used by the Climate Prediction Center/National Oceanic and Atmospheric Administration (CPC / NOAA), which used latitudes  $20^{\circ}\text{S}-90^{\circ}\text{S}$ . The poleward shift of the region analyzed here aimed to reduce tropical phenomena influence on the EOF calculation, such as El Niño-Southern Oscillation (ENSO) and AMM (Vasconcellos et al. 2019). The positive (negative) SAM index is associated with positive (negative) anomalies of geopotential height in the middle latitudes and negative (positive) anomalies in high latitudes (Thompson & Wallace 2000).

The monthly SASG index was constructed using SST anomalies in two different areas located in the Subtropical Atlantic Ocean, delimited as: northeastern area ( $20^{\circ}\text{S}-40^{\circ}\text{S}$ ;  $10^{\circ}\text{W}-40^{\circ}\text{W}$ ) and southwest area ( $40^{\circ}\text{S}-60^{\circ}\text{S}$ ;  $30^{\circ}\text{W}-60^{\circ}\text{W}$ ). The SASG index is defined by subtracting the SST in the southwestern area from the SST in the northeastern region. Positive SASG is associated with warmer SST in the northeastern part. This methodology is the same applied in Oliva et al. (2021).

According to Cavalieri & Parkinson (2008), the most extensive ASI extension occurs seasonally in September, with a climatological average of 17,500,000  $\text{km}^2$  to 18,900,000  $\text{km}^2$ . During this month, the

sea ice area exceeds the Antarctic continent area, which has approximately 14,000,000 km<sup>2</sup> (Wadhams 2000). We focus on the analysis for September because this month represents the climatological maximum for ASI extent. The climatological average from the 1981 to 2010 period was used as a reference. September climatology (1981-2010) of some variables were built to discuss this month's mean climate: 2m air temperature, precipitation, SLP, SST, and 250 hPa wind. The climatological extents of the entire ASI and WS sector (1981-2018) were also created.

A time series plot was constructed for September (1981-2018) to analyze the behavior of WS ice extent and the teleconnections patterns. Then, the correlation between each index (SAM, AMM, and SASG) and sea ice extent at each WS longitude was calculated and plotted in a graph. Boxplot diagrams were also prepared to analyze the performance of the WS ice extent for each of the four combinations between SAM and AMM (SAM positive/AMM negative, SAM positive/AMM positive, SAM negative/AMM negative, SAM negative/AMM positive); and between the SAM and the SASG (SAM positive/SASG negative, SAM positive/SASG positive, SAM negative/SASG negative, SAM negative/SASG positive).

As shown in our results and at Oliva et al. (2021), the negative SAM/positive AMM and negative SAM/positive SASG configurations were associated with maximum and minimum WS ice extent in September, respectively. Notably, the positive SAM/negative AMM combination had the most years of the lowest WS ice quintile (red in Table I). Likewise, the negative SAM/positive AMM combination had the most years of the highest WS ice quintile (green in Table I). The same can be found for positive SAM/negative SASG combination (red in Table I) and negative SAM/ positive SASG combinations (green in Table I), respectively.

After, the impacts of these modes' combinations (Table I) over South American climate were analyzed through composites of precipitation and 2m air temperature anomalies. A Student's t-test was applied on the climate composites (Wilks 2006) to determine regions within the 90% confidence level. Due to a short number of cases at each configuration, we decided to use confidence levels of 90%. A higher level of confidence excluded relevant information that is physically consistent with other analyses. This methodology was also used in previous papers (e.g., Vasconcellos & Cavalcanti 2010, Bernardino et al. 2018, Vasconcellos et al. 2019, Caldas et al. 2020).

To understand possible mechanisms associated with the combinations and South American climate, composites of anomalous streamline at 250 hPa and SST were performed. Composites of quasi-geostrophic stream function and the wave activity flux in 250 hPa were also calculated to identify the source of the atmospheric circulation anomalies. Takaya & Nakamura (2001) formulated the phase-independent wave activity flux applied to stationary and migratory waves. For this work, we are interested in stationary waves linked to variability modes and ASI, influencing the South American climate.

The phase-independent wave activity flux of Takaya & Nakamura (2001) can be formulated in cylindrical coordinates on the lat-lon plane as:

$$W = \frac{p \cos \Phi}{2 |U|} \left\{ \begin{array}{l} \frac{U}{a^2 \cos^2 \Phi} \left[ \left( \frac{\partial \Psi'}{\partial \lambda} \right)^2 - \Psi' \frac{\partial^2 \Psi'}{\partial \lambda^2} \right] + \frac{V}{a^2 \cos^2 \Phi} \left[ \frac{\partial \Psi'}{\partial \lambda} \frac{\partial \Psi'}{\partial \Phi} - \Psi' \frac{\partial^2 \Psi'}{\partial \lambda \partial \Phi} \right] \\ \frac{U}{a^2 \cos^2 \Phi} \left[ \frac{\partial \Psi'}{\partial \lambda} \frac{\partial \Psi'}{\partial \Phi} - \Psi' \frac{\partial^2 \Psi'}{\partial \lambda \partial \Phi} \right] + \frac{V}{a^2} \left[ \left( \frac{\partial \Psi'}{\partial \lambda} \right)^2 - \Psi' \frac{\partial^2 \Psi'}{\partial \lambda^2} \right] \end{array} \right\} + C_{UM} \quad (1)$$

Where U and V are the zonal mean of the zonal and meridional wind components, respectively;  $\Psi$  is the stationary component of 250-hPa stream function (e.g., with the subtraction the eulerian mean),

$\Phi$  is the latitude,  $\lambda$  is the longitude,  $a$  is the radius of the Earth,  $p$  the pressure level (250-hPa), and the quantities  $C_U$  and  $M$ , represent the phase velocity in the zonal direction and the pseudo-momentum (transfer of momentum by wave) for Quasi-Geostrophic eddies. The quantity  $C_U M$  gives us the effect of phase propagation (phase velocity) of the atmospheric wave. For the stationary waves, this term is zero.

**Table I. Years of the SAM/AMM and SAM/SASG combinations and years of maximum and minimum quintiles WS ice extent for 1981-2018. In green: maximum extreme quintile of sea ice in the WS. In red: minimum extreme quintile of sea ice in the WS. Adapted from Oliva et al. (2021).**

WEDDELL SEA - SEPTEMBER			
positive SAM / negative AMM	1982, 1984, 1985, 1986, 1992, 1993, 2018 (7)	positive SAM / negative SASG	1984, 1985, 1986, 1992, 1993, 2010, 2017, 2018 (8)
negative SAM / positive AMM	1981, 1987, 1988, 1989, 1991, 1996, 1998, 1999, 2003, 2005, 2006, 2007, 2009, 2011, 2013, 2014 (16)	negative SAM / positive SASG	1987, 1988, 1991, 1994, 2000, 2002, 2003, 2005, 2006, 2007, 2009, 2013 (12)

## RESULTS AND DISCUSSION

### September climatology

The September climatology (1981-2010) shows higher air temperature over lower latitudes, decreasing to higher latitudes (Figure 2a). On the continent, the greater values occur between Piauí and Goiás states. In western parts, lower values are founded over the Andes range. At the adjacent oceans, higher air temperature values, located in the tropical northern hemisphere, follow the SST values (Figure 3a). Negative air temperature occurs southward the continent, about 55°S.

For precipitation (Figure 2b), the climatology shows a maximum at approximately 10°-15°N, related to Intertropical Convergence Zone (ITCZ) position (e.g., Waliser & Gautier 1993, Melo et al. 2009). Over the continent, northwestern South America has the highest precipitation value, extending NW-SE into southern Amazonia. This configuration is typical of the pre-monsoon phase (Zhou & Lau 1998). Another maximum value is displayed over Southeastern South America, extending into South Atlantic. This maximum could be explained by cold fronts, which have their maximum frequency during austral spring over this area (Cavalcanti & Kousky 2009). The driest areas over the continent are over Northeastern Brazil, southern South America, and western subtropics. The last region is influenced by descending movements of the South Pacific Subtropical High (SPSH - Figure 2c). It includes the Atacama Desert, which is the driest globally (NATIONAL GEOGRAPHIC MAGAZINE 2003). The southern sector is leeward of the Andes, where the flow from the west that crosses the mountain range arrives dry in this region (Reboita et al. 2010). The SLP climatology (Figure 2c) shows the South Atlantic Subtropical High (SASH) and SPSH positions and the low-pressure belt at high latitudes. There is also the presence of the equatorial trough, extending into South America at a typical pre-monsoon configuration (Zhou & Lau 1998).

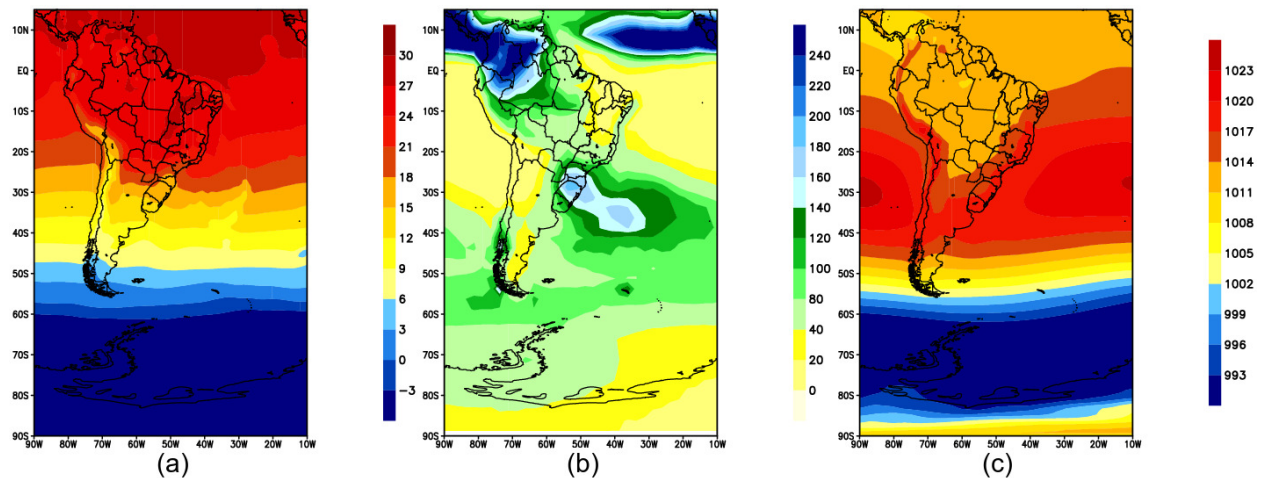


**Figure 2. September climatology (1981-2010): (a) air temperature ( $^{\circ}\text{C}$ ) (b) precipitation (mm); (c) Sea Level Pressure.**

The climatological SST shows higher values in the tropical northern hemisphere, coherent to oceans' thermal inertia, which delays the maximum temperature of boreal summer to the beginning of spring. The lowest values are found in polar regions. The influence of the prevailing ocean currents is seen along the eastern and western ocean basins and nearby coastal areas (Figure 3a). Over South America, the jet stream is located approximately between  $25^{\circ}$ - $45^{\circ}\text{S}$ . Also, the Bolivian High is visible.

The ASI has the minor average extension in February, both in the Southern Ocean, with 340.6 km, and in WS, with 705.2 km. On the other hand, September has the most significant average sea ice extension, with 1,245.1 km in the Southern Ocean and 1,906.4 km in WS (Figure 4a). These results agree with previous studies (e.g., King & Turner 1997, Wadhams 2000, Cavalieri & Parkinson 2008). Also, the WS sector has the most extensive sea ice coverage among the five sectors (Carpenedo 2017). These results justify the focusing of this paper on September and the WS sector.

### Relationship among WS ice extent and teleconnection pattern indexes

The September timeseries of WS ice extent and the teleconnections patterns indexes are seen in Figure 4b. There is interannual variability of WS ice extent relative to the climatology (Figure 4a). As expected, the SAM index (atmospheric pattern) presents more considerable interannual variability than AMM and SASG (oceanic indexes). The correlation of the WS ice extent with each index for each WS longitude is shown in Figure 4c. The correlation between WS ice extent and SAM is negative across the sector, with the highest value around  $30^{\circ}\text{W}$ . About the AMM index, the correlation is positive in almost the entire sector, with values at the limit of the WS sector with the Antarctic Peninsula, at  $60^{\circ}\text{W}$ . Concerned to SASG, the correlation coefficient with WS ice extent also is positive across the sector, with a maximum around  $25^{\circ}\text{W}$ . The AMM and SASG indexes correlations with WS ice are similar in most WS, except for regions between  $30^{\circ}$ - $45^{\circ}\text{W}$  and  $15^{\circ}\text{W}$ - $0^{\circ}$ . The SASG correlation with WS ice extent presents higher values in general. These results suggest these two patterns (AMM and SASG) have a synergy but are not part of the same system. Pezza et al. (2012) performed a similar correlation analysis, however, focusing 1979-2000, using all months and evaluating the SAM and ENSO indexes. The authors highlighted some areas of correlation between SAM and sea ice extent as west of WS (negative

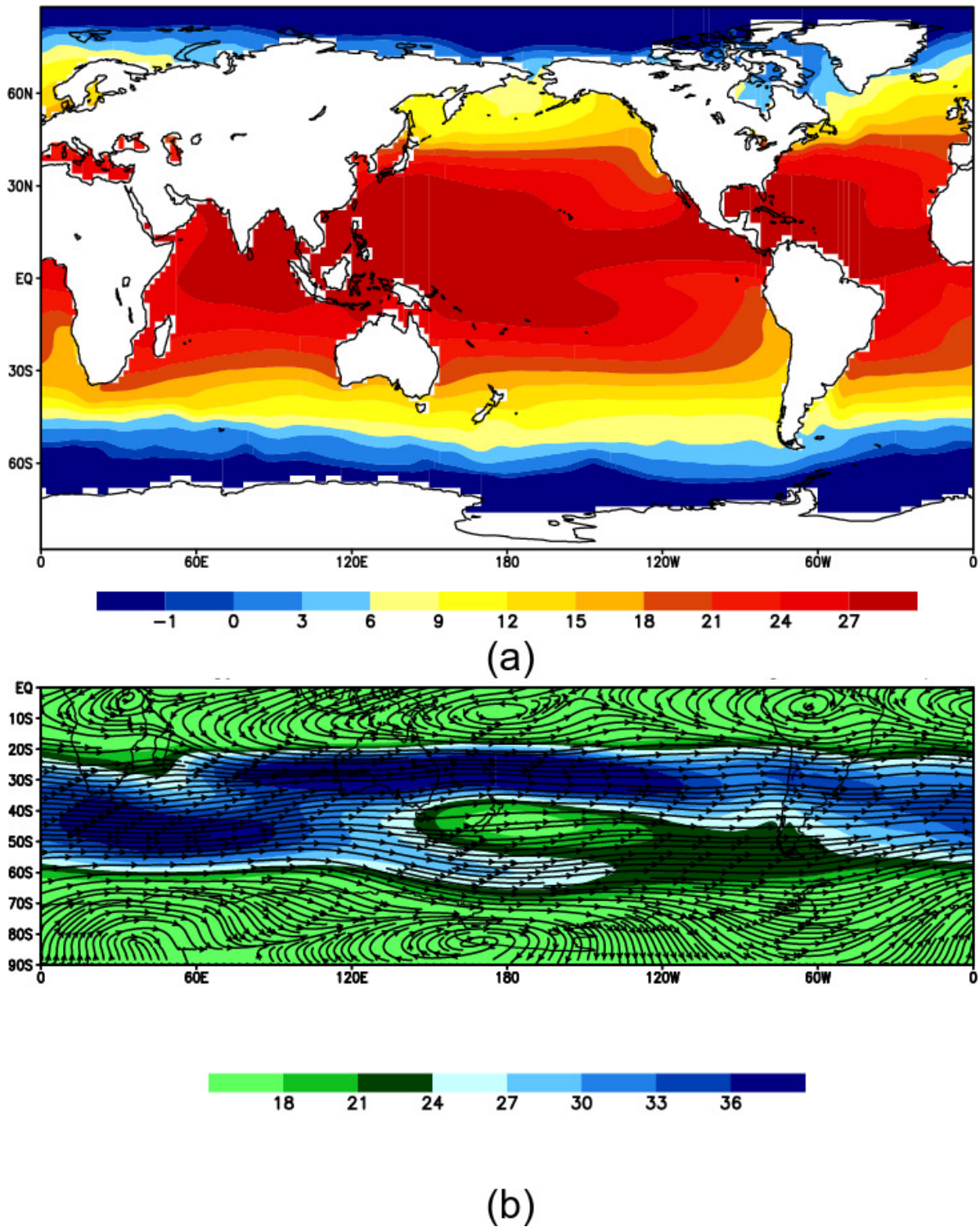


**Figure 3.** September climatology (1981-2010): (a) SST ( $^{\circ}\text{C}$ ); (b) Wind streamline and wind magnitude ( $\text{m.s}^{-1}$ ) at 250 hPa.

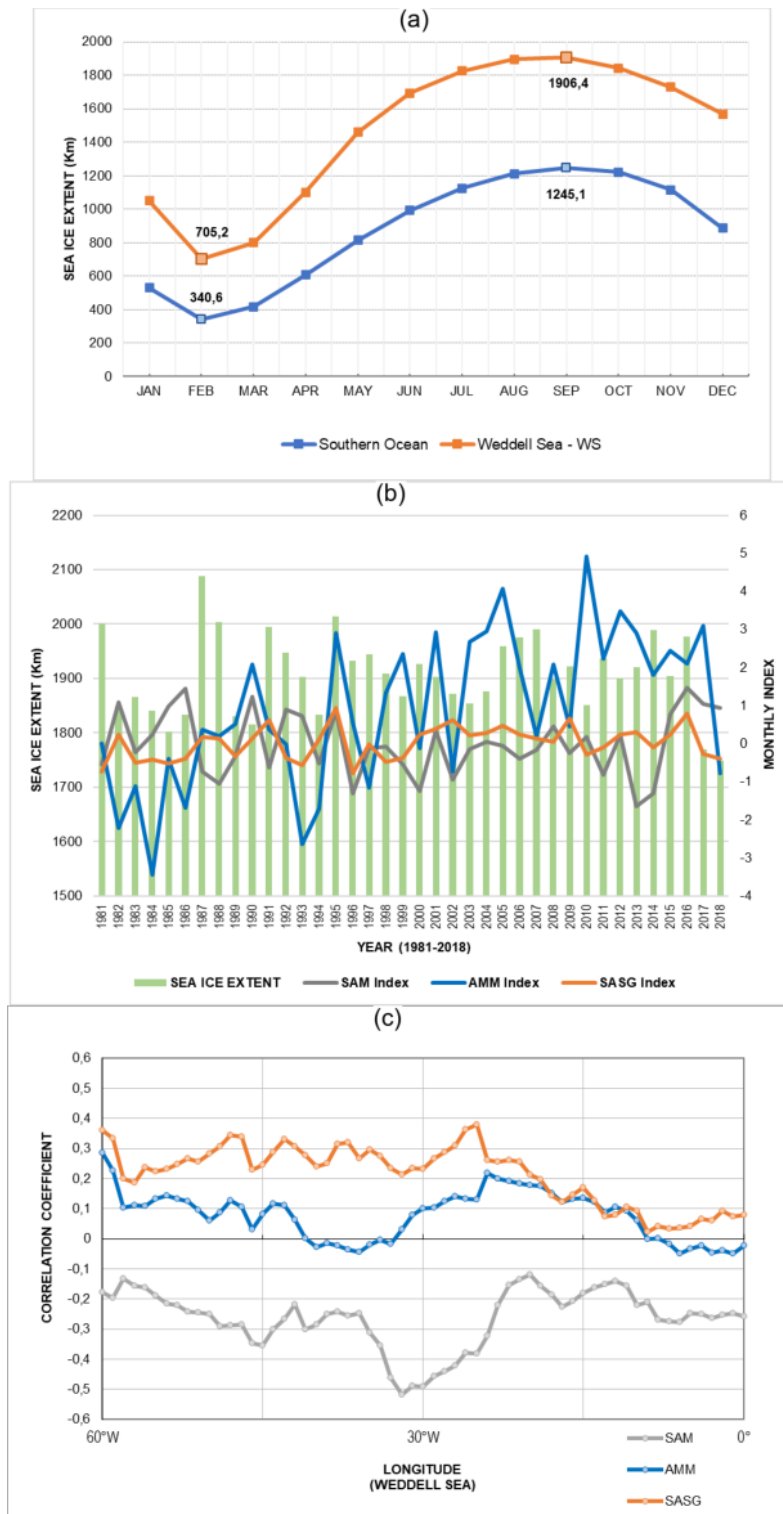


**Figure 4.** (a) Sea Ice extent (km) climatology (1981-2018) for all sectors (blue line) and for WS sector (orange line); (b) September time series of WS ice (km), SAM, AMM, and SASG indexes (1981-2018); (c) Correlation coefficients of the SAM (gray line), AMM (blue line), and SASG (orange line) indices with ice extent at each WS longitude.

correlation). According to the authors, sea ice retracts southward when westerlies more intense than usual occur.

The boxplot diagrams (Figure 5) show the behavior of the variability of sea ice extensions (minimum, maximum, 1st quartile, median and 3rd quartile), respectively, in the different phases of the SAM, AMM, and SASG patterns; in the four-phase combinations of the SAM and AMM phases (positive SAM/ negative AMM, positive SAM/positive AMM, negative SAM/ negative AMM, negative SAM/positive AMM – Figure 5a) and the four-phase combinations of the SAM and SASG phases (positive SAM/ negative SASG, positive SAM/positive SASG, negative SAM/ negative SASG, negative SAM/positive SASG

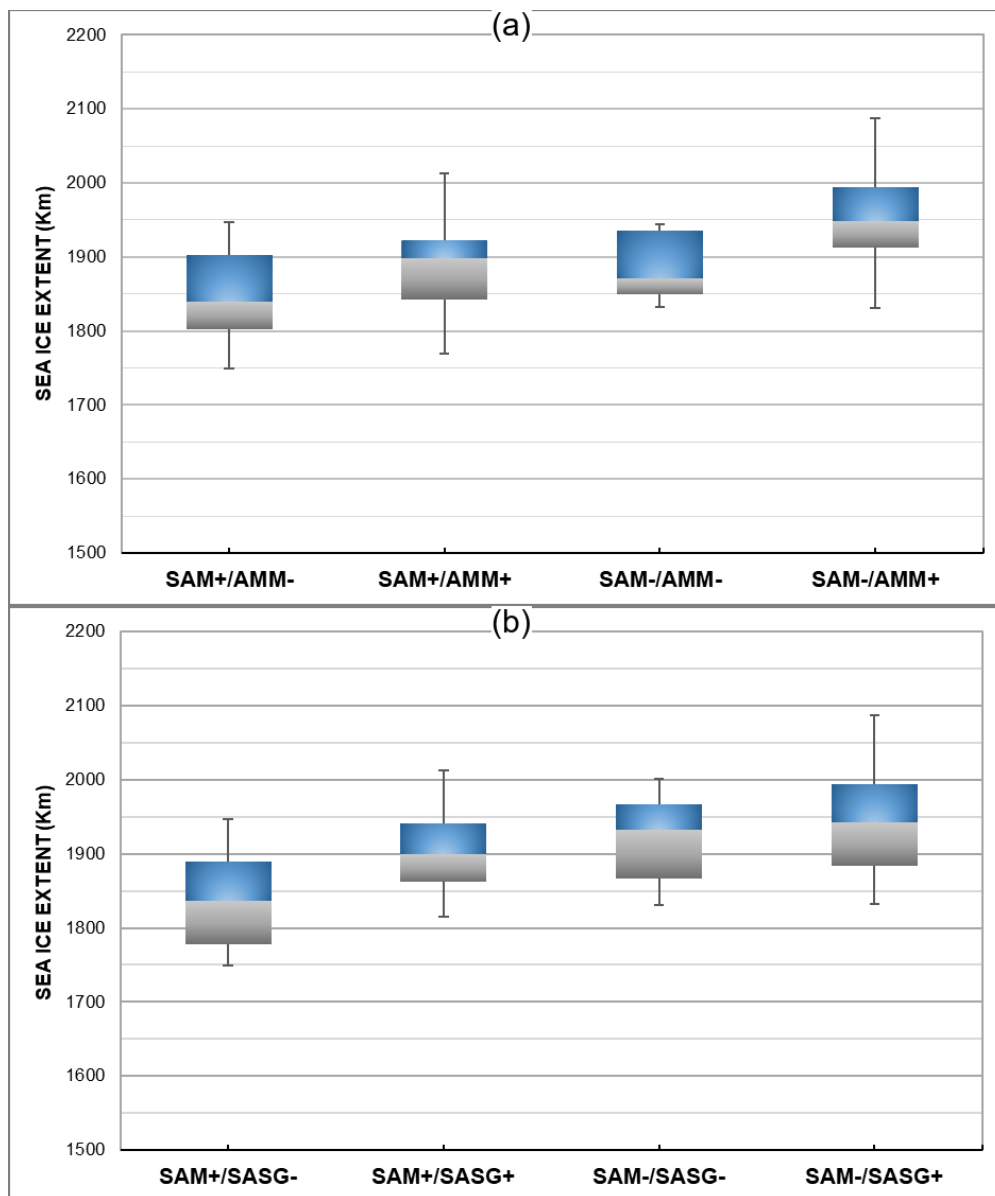


**Figure 5.** Boxplot diagram of WS ice extent for September (1981-2018): (a) for the four combinations of the SAM/AMM patterns, and (b) for the four combinations of the SAM/SASG patterns.

– Figure 5b). The highlight of the negative SAM/ positive AMM combination (Figure 5a) has the higher ice extent median, also having values in the 1st and 3rd quartiles higher than the other combinations. The smallest extension values occur in the inverse combination (positive SAM/ negative AMM). Figure 5b shows, in general, diagrams with similar ice extension behavior concerning the SAM/AMM diagrams. The most extensive combination is negative SAM/positive SASG. All values are superior to other combinations. The smallest values also occur in the inverse combination (positive SAM/ negative SASG).

### **The combined performance of WS ice extent, SAM, AMM, and SASG over the South American climate**

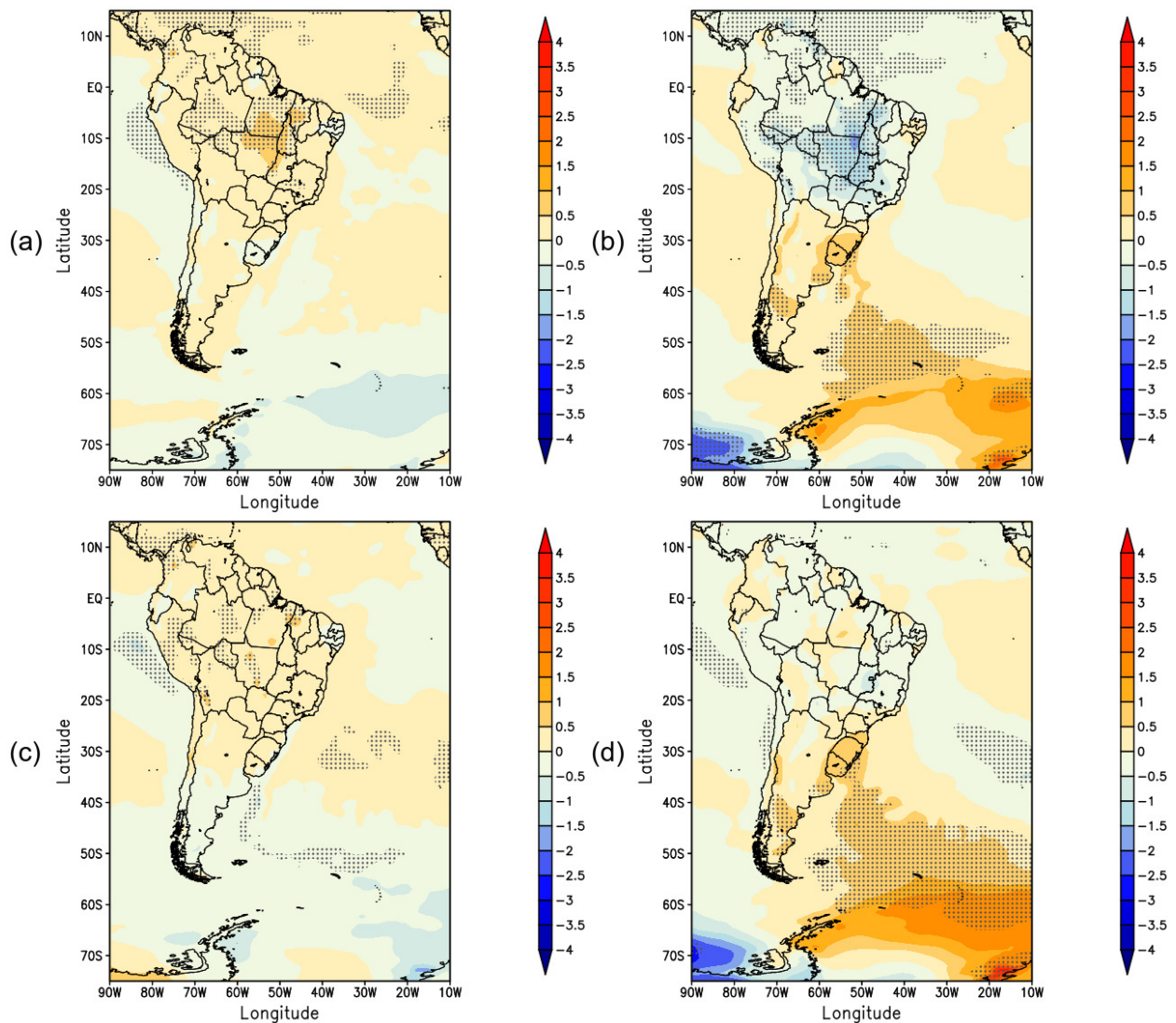
As the Oliva et al. (2021), the results presented above displayed which configurations of SAM and AMM phases and SAM and SASG phases are related to maximum and minimum WS ice extent: negative SAM/positive AMM phase and the negative SAM/positive SASG phase, associated with maximum WS ice extents, and the opposite combinations of these indices associated with minimum WS ice extents. Composites analysis for precipitation and 2m air temperature at South America and adjacent oceans were built for these configurations to analyze the combined impacts of these patterns and WS ice over South America.

Figure 6 presents the 2m air temperature composites for the combinations associated with the maximum and minimum WS ice extent (Table I). Figure 6a shows the temperature anomalies for the higher frequency of maximum sea ice extent occurrence (negative SAM/positive AMM) configuration. As expected, the composite related to the maximum WS ice extent presents negative temperature anomalies in the WS region and the Antarctic Peninsula, although without statistical significance. Over the tropical Atlantic, there are positive air temperature anomalies in the northern hemisphere – some areas with statistical significance – and negative anomalies in a 20°-10°S band, coherent with positive AMM phase. There is an alternation of air temperature anomalies between the WS and AMM regions, creating a positive anomaly over subtropics (approximately 50°-25°S). Meanwhile, in South America, positive air temperature anomalies are observed in almost the entire continent, reaching significant values above 1°C centered around 10°S and 55°W. These results agree with Morioka et al. (2017), that suggested low WS ice anomalies contribute to warmer skin temperature in the band of 60°-70°S.

For the lowest WS ice extent combination (positive SAM/negative AMM, Figure 6b), an opposite pattern is seen in tropical South America, with significant negative anomalies northward 25°S, reaching -2.0°C. The September minimum WS ice extent was associated with significant warm air anomalies at 2m from the WS region to South America. There seems to be a way for the climate signal meridional propagation, quite near the oceanic front of Brazil-Malvinas Confluence (Pezzi et al. 2009, Morioka et al. 2017). These results agree with Morioka et al. (2017), that suggested low WS ice anomalies contribute to warmer skin temperature in the band of 60°-70°S. Over the Atlantic, there are significant negative air temperature anomalies in the northern hemisphere. A positive signal is found over the central equatorial Atlantic, near the 30°-20°W longitude band. The cold (warm) anomalies found in this study over tropical South America and tropical North Atlantic occurred associated with the negative (positive) AMM phase, as shown in Figure 6b (Figure 6a). The negative AMM and the lowest WS ice extent at Figure 6b create an alternation of air temperature anomalies over the Atlantic with an approximately opposite signal found in Figure 6a. They also show that the Antarctic Dipole Mode (Yuan

& Martinson 2001) was excited in the maximum WS ice extent composite, which was established by cold (warm) anomalies in the west (east) side of the Antarctic Peninsula (Figure 6b). Also, for September, Vasconcellos et al. (2019) found a negative relationship between SAM and air temperature over part of the continent. Other studies also discussed the negative relation between SAM and WS ice extent (e.g., Pezza et al. 2008, 2012, Parise et al. 2015, Oliva et al. 2021).

The precipitation composites for the combinations associated with the maximum and minimum WS ice extent (Table I) are presented in Figure 7. As found in the air temperature field, there is an out-of-phase signal between negative SAM/positive AMM (associated with maximum sea ice extent – Figure 7a) and positive SAM/negative AMM (associated with minimum sea ice extent – Figure 7b)



**Figure 6.** Air temperature at 2m (°C) anomalies during September: (a) maximum sea ice in the WS sector, negative SAM, and positive AMM; (b) minimum sea ice in the WS sector, positive SAM, and negative AMM; (c) maximum sea ice in the WS sector, negative SAM, and positive SASG; (d) minimum sea ice in the WS sector, positive SAM, and negative SASG. Areas with a confidence level of 90% are dotted.

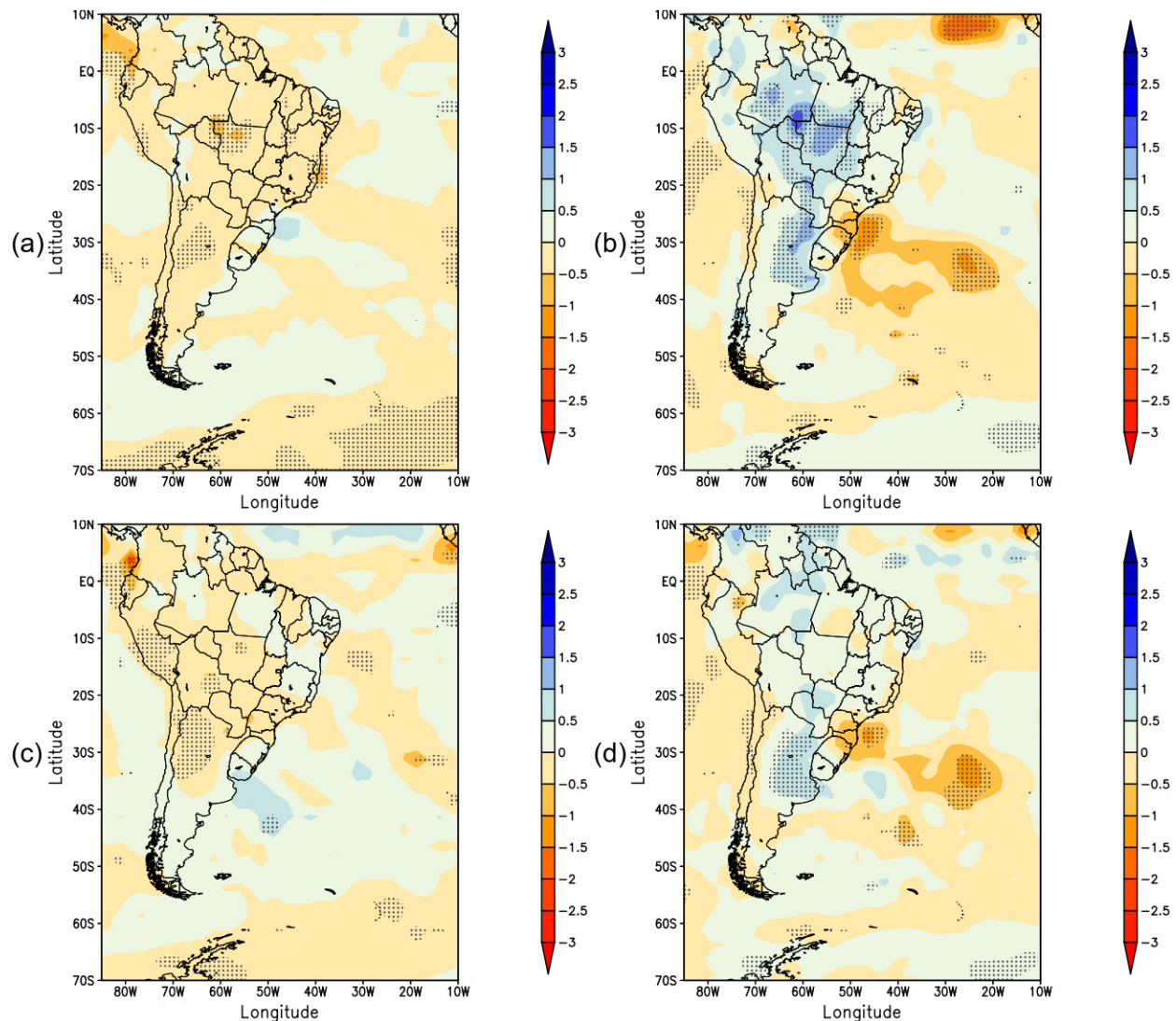


**Figure 7. Precipitation (mm) anomalies during September: (a) maximum sea ice in the WS sector, negative SAM, and positive AMM; (b) minimum sea ice in the WS sector, positive SAM, and negative AMM; (c) maximum sea ice in the WS sector, negative SAM, and positive SASG; (d) minimum sea ice in the WS sector, positive SAM, and negative SASG. Areas with a confidence level of 90% are dotted.**

phases. The Antarctic Peninsula and WS regions are drier (wetter) for the negative SAM/positive AMM (positive SAM/negative AMM) composite. The negative (positive) SAM phase could increase (decrease) geopotential over these regions, inhibiting (supporting) transient systems occurrence. Also, through the Clausius-Clapeyron equation (Wallace & Hobbs 2000), colder (warmer) atmosphere observed over these regions (Figure 6 a-b) support less (more) moisture, reinforcing the dryness (wetness). Almost all South America presents less (more) precipitation at negative SAM/positive AMM (positive SAM/negative AMM). The exception occurs mainly in Southern Brazil and Uruguay, which display an opposite configuration on the continent. These positive anomalies are connected to subtropical Atlantic ones. Vasconcellos et al. (2019) also found positive (negative) precipitation anomalies over most of the continent during the positive (negative) SAM phase and an inverse configuration over

Southern Brazil. But in their results, the extreme north of South America presented a similar signal to Southern Brazil. According to Cavalcanti & Kousky (2009), the highest frequency of cold fronts over most tropical South America occurs during spring. The results found here could indicate the cold fronts reaching southeastern South America at negative SAM/positive AMM, causing more precipitation over this region, but do not advance to continental lower latitudes, drying these northward regions. It agrees with Caldas et al. (2020), which indicated more frequency of cold fronts over Southeastern South America at the combination of negative SAM - El Niño - maximum WS ice extents. These results also indicate fewer South Atlantic Convergence Zone (SACZ) events or occurrence of the ocean-type SACZ (Carvalho et al. 2004). Rosso et al. (2018) suggested the frequency, persistence, and total precipitation of SACZ events were lower at the negative SAM phase. A teleconnection mechanism between the extratropics and the SACZ region is evident in positive SAM, through intensifying the polar and subtropical jets, in the days preceding SACZ. The same was not observed in the negative SAM phase, where the anomalies were confined in the subtropical region and displaced to the South Atlantic Ocean. Although the SACZ is not common in September, this month starts the wet period over part of the continent because of the maximum cold front occurrence. Thus, the dynamics processes discussed by Rosso et al. (2018) also be inferred this month. The positive (negative) AMM phase at Figure 7a (Figure 7b) also suggests a northward (southward) displacement of the ITCZ through wind-evaporation-SST (WES) feedback (e.g., Xie & Philander, 1994, Chiang et al. 2002, Vasconcellos et al. 2020), contributing with lower (higher) precipitation over the extreme northern South America. Therefore, the AMM could explain the differences between the precipitation composites and the Vasconcellos et al. (2019) over tropical South America.

Figures 6 c-d display the 2m air temperature composites for the SAM and SASG combinations associated with the maximum and minimum WS ice extent (Table I). The results are similar to SAM/AMM combinations (Figure 6 a-b). However, the impacts are different over southern Argentina. Colder (warmer) temperatures are observed at the negative SAM/positive SASG (positive SAM/negative SASG) – Figure 6c (Figure 6d). These signals extend into the adjacent Atlantic Ocean and are coherent to the positive (negative) SASG phase. Maximum (minimum) sea ice extent over WS also can be related to lower (higher) temperature at southern South Atlantic, and, consequently, with positive (negative) SASG phase.

As for temperature, the precipitation composites for SAM/SASG combinations (Figure 7 c-d) are like SAM/AMM ones (Figure 7 a-b). These similarities suggest the Atlantic Ocean pattern (AMM and SASG) are in synergy, although these patterns act in different regions (tropics and subtropics/extratropics, respectively).

### **Possible links among the WS ice extent, SAM, AMM, SASG, and the South American climate**

To understand the link among these variability modes, the WS ice extent, and the South American climate presented in the previous section, we analyzed composites of anomaly circulation and the wave activity flux at high levels. Composites of anomaly streamline at 250 hPa are presented in Figures 8 (a-b) and 9 (a-b). The maximum sea ice extent occurrence (negative SAM/positive AMM) configuration shows a high level anomalous cyclonic circulation over the Southern Cone of South America, extending southeastward to the Atlantic (Figure 8a). It could explain the warmer and dryness conditions over most of the continent (Figures 6a and 7a, respectively). Over the tropical Atlantic, there

is an anomalous anticyclonic circulation northeastward of the continent's cyclonic center that could explain some regions of positive anomalous precipitation over the Atlantic. The negative geopotential anomalies at middle latitudes, related to the negative SAM phase, explain the anomaly cyclonic circulations presented at most of this belt. A wavenumber three at middle and high latitudes and wavetrains triggered from the Indian Ocean and eastward of New Zealand could explain the position of the anomalous cyclonic over South America and the anticyclonic one northward the continent. The wave flux activity (Figure 8c) shows the wave flux associated with both wavetrains, including cyclonic activity flux over the Southern Cone of South America. The quasi-geostrophic stream function is in agreement with negative SAM phase.

For minimum sea ice extent configuration (positive SAM/ negative AMM), there is a high level anomalous anticyclonic circulation over Southern Cone of South America and adjacent Atlantic Ocean (Figure 8b), explaining the colder and wetter continent (Figures 6b and 7b, respectively). Morioka et al. (2017) also found low WS ice concentrations are strongly associated with anticyclonic atmospheric circulation anomalies in the South Atlantic. Also, there is an anomalous cyclonic circulation over the Atlantic, northward the cyclonic one, which could explain the dryness region eastward of Southeastern South America. The positive geopotential anomalies at middle latitudes (positive SAM phase) explain the anticyclonic anomaly circulations presented at most of this belt. These anomalous circulations over South America are also associated with wavetrains, but they started at the western Pacific and the Indian Ocean, southwestward Australia. The quasi-geostrophic stream function confirms the positive SAM phase, while the wave flux activity (Figure 8 d) ratifies the wavetrains, including anticyclonic activity flux over Southern South America. It is noteworthy that the wave activity flux is more intense at this configuration than the maximum sea ice extent configuration (Figure 8c).

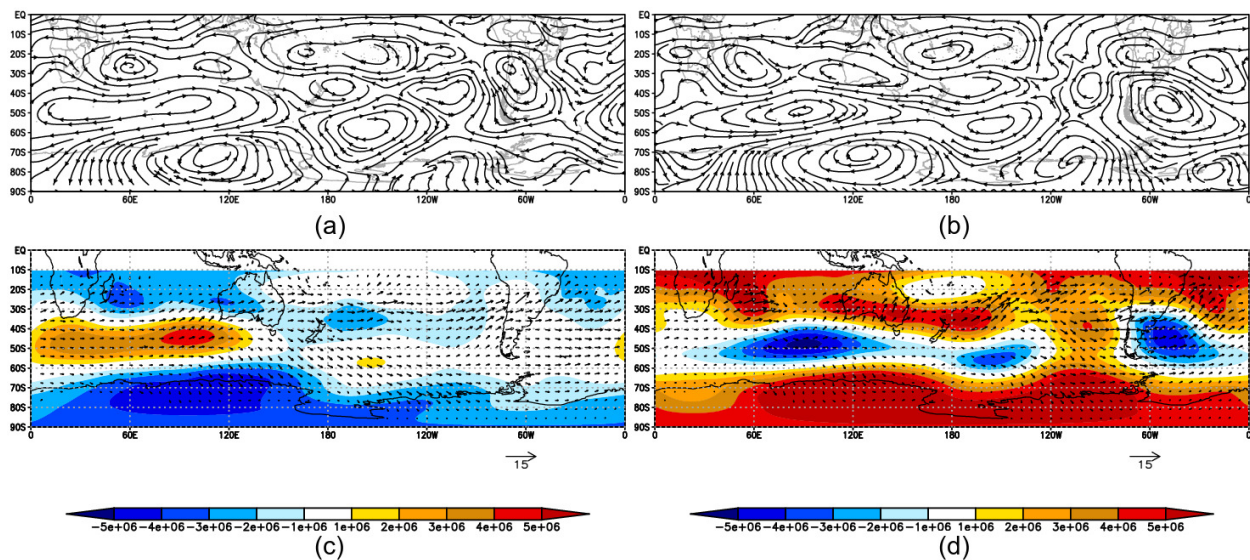


**Figure 8.** (a, b) wind anomaly streamlines at 250 hPa; (c,d) anomalous quasi-geostrophic stream function ( $m^2.s^{-1}$  - shaded) and wave activity flux ( $m^2.s^{-2}$  - arrows - define by Takaya & Nakamura (2001). Left side (a, c): maximum sea ice in the WS sector, negative SAM, and positive AMM. Right side (b, d): minimum sea ice in the WS sector, positive SAM, and negative AMM.

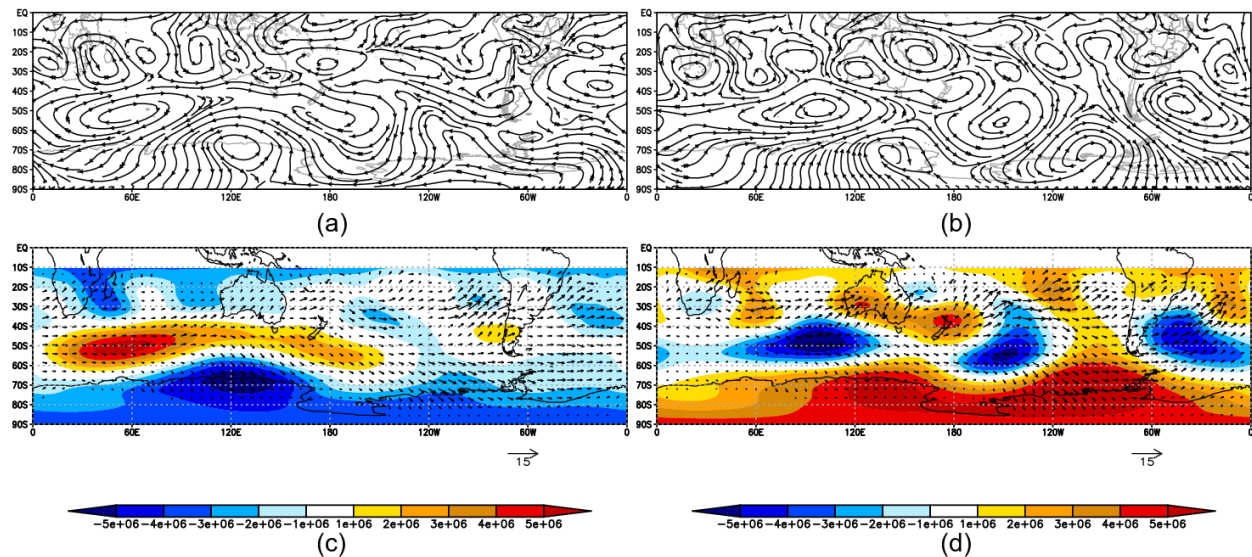


**Figure 9.** (a, b) wind anomaly streamlines at 250 hPa; (c,d) anomalous quasi-geostrophic stream function ( $m^2 \cdot s^{-1}$  - shaded) and wave activity flux ( $m^2 \cdot s^{-2}$  - arrows - define by Takaya & Nakamura (2001). Left side (a, c): maximum sea ice in the WS sector, negative SAM, and positive SASG. Right side (b, d): minimum sea ice in the WS sector, positive SAM, and negative SASG.

As for SAM/AMM (Figure 8a), SAM/SASG configurations for maximum WS ice extent (negative SAM/positive SASG) presents, over the continent, anomalous cyclonic circulations at Southern Cone, and an anomalous anticyclonic circulation over the Atlantic (Figure 9a). However, the circulations over the continent are not broader as in the SAM/AMM. It could explain the warm and dry conditions over most of the continent, but with a cold and wet situation over southern South America. Over the ocean, the anomalous anticyclonic circulation is larger and southward than in SAM/AMM, causing a larger area of wetter conditions over the Atlantic. These anomalous circulations are related to wavetrains triggered at the western Indian Ocean, near Madagascar, and the central Pacific (Figure 9a). The anomaly circulation (Figure 9a) and quasi-geostrophic stream function (Figure 9c) confirm the positive SAM phase. The wave flux activity (Figure 9c) corroborates the wavetrains and a lower cyclonic flux activity to southern South America (Figure 9a).

The positive SAM/negative SASG (minimum sea ice extent) also presents a high-level anomalous anticyclonic circulation but displaced to the Atlantic, reaching only Southern South America (Figure 9b). There is an anomalous cyclonic circulation over the Atlantic, northward the cyclonic circulation (Figure 9b), and consequently, also more displaced to the ocean than the SAM/AMM one (Figure 9a). Likewise, these circulations are related to wavenumber three at middle and high latitudes and wavetrains triggered from the Indian Ocean and eastward of New Zealand. As in the other cases, the stream function shows the SAM phase (Figure 9d). The wave flux activity ratifies the similarity with SAM/AMM configuration, but with the SASG displacing the flux eastward the continent, over the Atlantic Ocean (Figure 9d).

## CONCLUSIONS

This paper analyzed the relationships among tropical (AMM), subtropical (SASG), and extratropical (SAM) teleconnection patterns, the WS ice extent, and the South American climate variability through composites analysis for the configurations associated with a higher occurrence of maximum and minimum WS ice extents. When combining SAM/AMM phases and SAM/SASG phases, the largest extent of WS ice is found in the following configurations: negative SAM/ positive AMM and the negative SAM/positive SASG. The opposite combinations are associated with minimum WS ice extents. These configurations related to maximum and minimum WS ice extents are according to Oliva et al. (2021). The goal was to understand the combined impacts of these teleconnection patterns linked to WS ice extent over South American climate.

Negative SAM/positive AMM and negative SAM/positive SASG composites, both related to maximum WS ice extent (positive SAM/negative AMM and positive SAM/negative SASG, both related to minimum WS ice extent), are similar, mainly over tropical South America. Negative (positive) air temperature anomalies are present in the WS region and the Antarctic Peninsula in the maximum (minimum) WS ice extent combinations. For South America, positive air temperature anomalies are observed in a significant part of the continent for maximum WS ice extent combinations, with an opposite signal at tropical South America for minimum WS ice extent combinations. The anomalies over the northern part of South America agree with the AMM phases. Over Southern Argentina, colder (hotter) temperatures are observed at the negative SAM/positive SASG (positive SAM/negative SASG), influenced by positive (negative) SASG phase and maximum (minimum) sea ice extent over WS. Vasconcellos et al. (2019) also found a negative relationship between SAM and air temperature over part of the continent during September. Over South America, there is less (more) precipitation at maximum (minimum) WS ice extent combinations. The exception occurs in Southern Brazil and Uruguay, which display an opposite configuration of the rest of the continent.

Circulation and wave activity flux were analyzed to understand the link among these variability modes, the WS ice extent, and the South American climate. The anomalous anticyclonic (cyclonic) belt at middle latitude, typical of positive (negative) SAM phase, was seen at the composites, including over South America. Wavetrains from different regions of the Pacific and Indian Oceans modulated the position of high-level anomalous cyclonic (anticyclonic) circulation over the continent at maximum (minimum) WS ice extent configuration, which explains the drier and warmer (wetter and colder) results. The relation between wavetrains like-PSA and SAM was explored by previous authors (e.g., Vasconcellos & Cavalcanti 2010). The AMM signal extends the signal of temperature and precipitation to the northern part of South America. For SAM/SASG composites, the SASG signal was responsible for displacing the anomaly circulations eastward from South America, impacting more of the adjacent Atlantic. The wave flux activity corroborated the role of wavetrains, SAM, and SASG at the circulation anomalies and, consequently, to precipitation and temperature anomalies over South America.

Our study concluded that the SAM, AMM, and SASG modes and WS ice extent act synergically over the South American climate variability.

## Acknowledgments

The authors would like to thank the funding support of Conselho Nacional de Desenvolvimento Científico e Tecnológico (CNPq) for the Ph.D. scholarship granted to Fabio Oliva and the Project “Antarctic Modeling Observation System – ATMOS” (Process 443013/2018-7).

## REFERENCES

- ADLER RF ET AL. 2003. The version-2 global precipitation climatology project (GPCP) monthly precipitation analysis (1979–present). *J hydrometeorol* 4(6): 1147-1167.
- BERNARDINO BS, VASCONCELLOS FC & NUNES AM. 2018. Impact of the equatorial Pacific and South Atlantic SST anomalies on extremes in austral summer precipitation over Grande river basin in Southeast Brazil. *Int J Climatol* 38: e131-e143.
- BOMBARDI RJ, CARVALHO L & JONES C. 2014. Simulating the influence of the South Atlantic dipole on the South Atlantic convergence zone during neutral ENSO. *Theor Appl Climatol* 118(1): 251-269.
- BUDD W, GORDON A, HEMPEL G, LORIUS C & WELLER G. 1989. The role of Antarctica in global change. *Polar Record*, Prepared by the Steering Committee for the IGBP. ICSU Press/SCAR, 28 p.
- CALDAS CFD, VASCONCELLOS FC, CAVALCANTI IFDA, DE CARVALHO NO & LOPES IDR. 2020. Impact of Antarctic Sea Ice, ENOS, and Southern Annular Mode on Cold Fronts in South America. *Anu Inst Geociênc* 43(4): 229-237.
- CARPENEDO C. 2017. Bloqueios atmosféricos associados à variabilidade extrema do gelo marinho antártico e impactos na América do Sul. Ph.D. thesis. São Paulo University.
- CARPENEDO CB & AMBRIZZI T. 2016. Células de circulação meridional durante os eventos extremos de gelo marinho antártico. *Rev Bras Meteorol* 31: 251-261.
- CARPENEDO C, AMBRIZZI T & AÍMOLA L. 2013. Possíveis relações entre a variabilidade interanual do gelo marinho antártico e a precipitação na América do Sul. *Ciênc Nat*, p. 87-89.
- CARVALHO LM, JONES C & AMBRIZZI T. 2005. Opposite phases of the Antarctic Oscillation and relationships with intraseasonal to interannual activity in the tropics during the austral summer. *J Clim* 18(5): 702-718.
- CARVALHO LM, JONES C & LIEBMANN B. 2004. The South Atlantic convergence zone: Intensity, form, persistence, and relationships with intraseasonal to interannual activity and extreme rainfall. *J Clim* 17(1): 88-108.
- CAVALCANTI IFA & KOUSKY V. 2009. Frentes Frias sobre o Brasil. In: Cavalcanti I, Ferreira N, MGAJ S & MAFS D (Eds), *Tempo e Clima no Brasil*. p. 135-147. São Paulo: Oficina de textos.
- CAVALIERI D & PARKINSON C. 2008. Antarctic sea ice variability and trends, 1979-2006. *J Geophys Res Oceans* 113(C7).
- CHIANG JC, KUSHNIRY & GIANNINI A. 2002. Deconstructing Atlantic Intertropical Convergence Zone variability: Influence of the local cross-equatorial sea surface temperature gradient and remote forcing from the eastern equatorial Pacific. *J Geophys Res Atmos* 107(D1): ACL-3.
- CHIANG JC & VIMONT DJ. 2004. Analogous Pacific and Atlantic meridional modes of tropical atmosphere-ocean variability. *J Clim* 17(21): 4143-4158.
- CLEM KR & FOGT RL. 2013. Varying roles of ENSO and SAM on the Antarctic Peninsula climate in austral spring. *J Geophys Res Atmos* 118(20): 11-481.
- CLEM KR, RENWICK JA, MCGREGOR J & FOGT RL. 2016. The relative influence of ENSO and SAM on Antarctic Peninsula climate. *J Geophys Res Atmos* 121(16): 9324-9341.
- COMISO J. 2017. Bootstrap Sea Ice Concentrations from Nimbus-7 SMMR and DMSP SSM/I-SSMIS. NASA National Snow and Ice Data Center Distributed Active Archive Center.
- COMISO JC, GERSTEN RA, STOCK LV, TURNER J, PEREZ GJ & CHO K. 2017. Positive trend in the Antarctic sea ice cover and associated changes in surface temperature. *J Clim* 30(6): 2251-2267.
- CUNNINGHAM CA & BONATTI JP. 2011. Local and remote responses to opposite Ross Sea ice anomalies: a numerical experiment with the CPTec/INPE AGCM. *Theor Appl Climatol* 106(1): 23-44.
- DEE DP ET AL. 2011. The ERA-Interim reanalysis: Configuration and performance of the data assimilation system. *Q J R Meteorol Soc* 137(656): 553-597.
- FAUCHEREAU N, TRZASKA S, RICHARD Y, ROUCOU P & CAMBERLIN P. 2003. Sea-surface temperature co-variability in the Southern Atlantic and Indian Oceans and its connections with the atmospheric circulation in the Southern Hemisphere. *Int J Climatol: A Journal of the Royal Meteorological Society* 23(6): 663-677.

- FOGT RL & MARSHALL GJ. 2020. The Southern Annular Mode: variability, trends, and climate impacts across the Southern Hemisphere. *Wiley Interdisciplinary Reviews: Clim Change* 11(4): e652.
- GLOERSEN P, CAMPBELL W, CAVALIERI D, COMISO J, PARKINSON C & ZWALLY H (Eds). 1992. Arctic and Antarctic sea ice, 1978-1987: Satellite passive-microwave observations and analysis. NASA. (NASA Special publication, 511), 290 p.
- HALL A & VISBECK M. 2002. Synchronous variability in the Southern Hemisphere atmosphere, sea ice, and ocean resulting from the annular mode. *J Clim* 15(21): 3043-3057.
- HERMES J & REASON C. 2005. Ocean model diagnosis of interannual coevolving SST variability in the South Indian and South Atlantic Oceans. *J Clim* 18(15): 2864-2882.
- HUANG B, THORNE PW, BANZON VF, BOYER T, CHEPURIN G, LAWRIMORE JH, MENNE MJ, SMITH TM, VOSE RS & ZHANG HM. 2017. Extended reconstructed sea surface temperature, version 5 (ERSSTv5): upgrades, validations, and intercomparisons. *J Clim* 30(20): 8179-8205.
- JORGETTI T, SILVA DIAS PL & FREITAS ED. 2014. The relationship between South Atlantic SST and SACZ intensity and positioning. *Clim Dyn* 42(11): 3077-3086.
- KING J & TURNER J. 1997. Antarctic meteorology and climatology. University Press, 409 p.
- LEFEBVRE W & GOOSSE H. 2005. Influence of the Southern Annular Mode on the sea ice-ocean system: the role of the thermal and mechanical forcing. *Ocean Sci* 1(3): 145-157.
- LIMA FUFU & CARVALHO LM. 2017. Mechanisms associated with winter intraseasonal extreme sea ice extent in the Weddell Sea. *Adv Polar Sci* 3: 171-184.
- MELO A, CAVALCANTI I & SOUZA P. 2009. Zona de Convergência Intertropical do Atlântico. In: Cavalcanti I, Ferreira N, MGAJ S & MAFS D (Eds), *Tempo e Clima no Brasil*. p. 25-41. São Paulo: Oficina de textos.
- MORIOKA Y, TOZUKA T & YAMAGATA T. 2011. On the growth and decay of the subtropical dipole mode in the South Atlantic. *J Clim* 24(21): 5538-5554.
- MORIOKA Y, ENGELBRECHT F & BEHERA SK. 2017. Role of Weddell Sea ice in South Atlantic atmospheric variability. *Clim Res* 74(2): 171-184.
- NATIONAL GEOGRAPHIC MAGAZINE. 2003. The driest place on earth. <http://ngm.nationalgeographic.com/ngm/0308/feature3/index.html>.
- OLIVA FG, VASCONCELLOS FC, DA SILVA TM & PIZZOCHERO RM. 2021. Extremos de Gelo Marinho Antártico no Mar de Weddell e Relações com Padrões de Teleconexões Climáticas. *Rev Bras Geogr Fis* 14(04): 2253-2268.
- PARISE CK, PEZZI LP, HODGES KI & JUSTINO F. 2015. The Influence of Sea Ice Dynamics on the Climate Sensitivity and Memory to Increased Antarctic Sea Ice. *J Clim* 28(24): 9642-9668.
- PEZZA AB, DURRANT T, SIMMONDS I & SMITH I. 2008. Southern Hemisphere synoptic behavior in extreme phases of SAM, ENSO, sea ice extent, and southern Australia rainfall. *J Clim* 21(21): 5566-5584.
- PEZZA AB, RASHID HA & SIMMONDS I. 2012. Climate links and recent extremes in Antarctic sea ice, high-latitude cyclones, Southern Annular Mode and ENSO. *Clim Dyn* 38(1): 57-73.
- PEZZI LP, DE SOUZA RB, ACEVEDO O, WAINER I, MATA MM, GARCIA CA & DE CAMARGO R. 2009. Multiyear measurements of the oceanic and atmospheric boundary layers at the Brazil-Malvinas confluence region. *J Geophys Res Atmos* 114(D19).
- RAPHAEL M, HOBBS W & WAINER I. 2011. The effect of Antarctic sea ice on the Southern Hemisphere atmosphere during the southern summer. *Clim Dyn* 36(7): 1403-1417.
- REBOITA MS, AMBRIZZI T & ROCHA RPD. 2009. Relationship between the southern annular mode and southern hemisphere atmospheric systems. *Rev Bras Meteorol* 24(1): 48-55.
- REBOITA MS, GAN MA, ROCHA RPD & AMBRIZZI T. 2010. Regimes de precipitação na América do Sul: uma revisão bibliográfica. *Rev Bras Meteorol* 25: 185-204.
- ROSSO FV, BOIASKI NT, FERRAZ SET & ROBLES TC. 2018. Influence of the Antarctic oscillation on the South Atlantic convergence Zone. *Atmosphere* 9(11): 431.
- SILVESTRI G & VERA C. 2009. Nonstationary impacts of the southern annular mode on Southern Hemisphere climate. *J Clim* 22(22): 6142-6148.
- STERL A & HAZELEGER W. 2003. Coupled variability and air-sea interaction in the South Atlantic Ocean. *Clim Dyn* 21(7): 559-571.
- TAKAYA K & NAKAMURA H. 2001. A formulation of a phase-independent wave-activity flux for stationary and migratory quasigeostrophic eddies on a zonally varying basic flow. *J Atmos Sci* 58(6): 608-627.
- THOMPSON DW & WALLACE JM. 2000. Annular modes in the extratropical circulation. Part I: Month-to-month variability. *J Clim* 13(5): 1000-1016.

VASCONCELLOS FC & CAVALCANTI IF. 2010. Extreme precipitation over Southeastern Brazil in the austral summer and relations with the Southern Hemisphere annular mode. *Atmos Sci Lett* 11(1): 21-26.

VASCONCELLOS FC, DENG Y, ZHANG H & MARTINS G. 2020. Austral Summer Precipitation Biases Over Tropical South America in Five Cmp5 Earth System Models. *Int J Climatol* 40(15): 6506-6525. doi:10.1002/joc.6595.

VASCONCELLOS FC, PIZZOCHERO RM & CAVALVANTI IFDA. 2019. Month-to-month impacts of Southern annular mode over South America climate. *Anu Inst Geociênc* 42(1): 783-792.

VASCONCELLOS FC & SOUZA JND. 2022. The anomalous wet 2020 southeast Brazil austral summer: characterization and possible mechanisms. *Atmosfera* 35(1): 27-38.

VENEGAS SA, MYSAK LA & STRAUB DN. 1997. Atmosphere–Ocean Coupled Variability in the South Atlantic. *J Clim* 10(11): 2904-2920. doi:10.1175/1520-0442(1997)010<2904:AOCVIT>2.0.CO;2.

WADHAMS P. 2000. *Ice in the ocean*. Gordon and Breach Science Publishers, 351 p.

WAINER I, PRADO L, KHODR IM & OTTO-BLIESNER B. 2014. Reconstruction of the south atlantic subtropical dipole index for the past 12000 years from surface temperature proxy. *Sci Rep* 4(1): 1-8.

WALISER DE & GAUTIER C. 1993. A satellite-derived climatology of the ITCZ. *J Clim* 6(11): 2162-2174.

WALLACE J & HOBBS P. 2000. *Atmospheric science: An introductory survey*. Elsevier Academic Press, 483 p.

WILKS D. 2006. *Statistical methods in the atmospheric sciences*. Academic Press (International Geophysics Series 91), 627 p.

XIE S & PHILANDER SGH. 1994. A coupled ocean-atmosphere model of relevance to the ITCZ in the eastern Pacific. *Tellus A* 46(4): 340-350.

YUAN X & MARTINSON DG. 2001. The Antarctic dipole and its predictability. *Geophys Res Lett* 28(18): 3609-3612.

ZHOU J & LAU KM. 1998. Does a monsoon climate exist over South America? *J Clim* 11(5): 1020-1040.

*Manuscript received on June 1, 2021;*  
*accepted for publication on January 13, 2022*

**FERNANDA C. VASCONCELLOS<sup>1</sup>**  
<https://orcid.org/0000-0002-5931-1503>

**FÁBIO G. OLIVA<sup>2</sup>**  
<https://orcid.org/0000-0003-4703-2862>

**RENAN M. PIZZOCHERO<sup>4</sup>**  
<https://orcid.org/0000-0002-1723-2655>

**TELMA M. DA SILVA<sup>2</sup>**  
<https://orcid.org/0000-0002-8295-6158>

**CLÁUDIA K. PARISE<sup>3</sup>**  
<https://orcid.org/0000-0002-9466-788X>

**CATHARINE F. DE CALDAS<sup>1</sup>**  
<https://orcid.org/0000-0003-3970-1325>

<sup>1</sup>Grupo de Estudos, Previsões e Análises Climáticas (GEPAC), Departamento de Meteorologia, Universidade Federal do Rio de Janeiro (UFRJ), Av. Athos da Silveira Ramos, 274, Cidade Universitária, 21941-916 Rio de Janeiro, RJ, Brazil

<sup>2</sup>Programa de Pós-Graduação em Geografia (PPGG), Universidade Federal do Rio de Janeiro (UFRJ), Av. Athos da Silveira Ramos, 274, Cidade Universitária, 21941-916 Rio de Janeiro, RJ, Brazil

<sup>3</sup>Laboratório de Estudos de Oceanografia Geológica (LEOG), Departamento de Oceanografia e Limnologia, Universidade Federal do Maranhão (UFMA), Avenida dos Portugueses, 1966, 65080-805 São Luís, MA, Brazil

<sup>4</sup>Instituto Nacional de Pesquisas Espaciais (INPE), Rodovia Presidente Dutra, Km 39, 12630-000 Cachoeira Paulista, SP, Brazil

Correspondence to: **Fernanda Cerqueira Vasconcellos**

*E-mail: fernandavasconcellos@igeo.ufrj.br*

### Author contributions

Fernanda Vasconcellos – advisor, helped to discuss the achieved results and wrote the manuscript. Fabio Oliva – this paper contains part of his doctorate research; helped to create and discuss the achieved results. Telma Silva – advisor, helped to discuss the achieved results. Claudia Parise – helped to discuss the achieved results. Renan Pizzochero – helped to create and discuss the achieved results. Catharine Caldas – helped to create the achieved results.

### How to cite

VASCONCELLOS FC, OLIVA FG, PIZZOCHERO RM, DA SILVA TM, PARISE CK & DE CALDAS CF. 2022. Combined performance of September's Weddell sea ice extent, Southern Annular Mode, and Atlantic SST anomalies over the South American temperature and precipitation. *An Acad Bras Cienc* 94: e20210803. DOI 10.1590/0001-376520220210803.

